

We are IntechOpen, the world's leading publisher of Open Access books Built by scientists, for scientists

6,900

Open access books available

185,000

International authors and editors

200M

Downloads

Our authors are among the

154

Countries delivered to

TOP 1%

most cited scientists

12.2%

Contributors from top 500 universities



WEB OF SCIENCE™

Selection of our books indexed in the Book Citation Index
in Web of Science™ Core Collection (BKCI)

Interested in publishing with us?
Contact book.department@intechopen.com

Numbers displayed above are based on latest data collected.
For more information visit www.intechopen.com



TiO₂- and ZnO-Based Materials for Photocatalysis: Material Properties, Device Architecture and Emerging Concepts

Olga M. Ishchenko, Vincent Rogé,
Guillaume Lamblin and Damien Lenoble

Additional information is available at the end of the chapter

<http://dx.doi.org/10.5772/62774>

Abstract

Numerous kinds of photocatalysts such as oxide-, nitride- or sulfide-based semiconductors, conducting polymers or graphene oxide-based materials have emerged since the discovery of water splitting on TiO₂ electrodes in 1972. Yet, metal-oxides are still largely the main family of materials promoted into photocatalytic applications.

In this chapter, we focus on the application of supported nanostructures of metal oxides, principally TiO₂ and ZnO, for the heterogeneous photocatalysis. We emphasize the benefits of increasing the specific surface area by using the direct growth of metal-oxide nanostructures onto porous templates. Among the numerous strategies to improve the photocatalytic activity, we detail the fabrication of semiconductor metal-oxide heterostructures promoting the charge separation under UV irradiation. We also describe how the use of plasmonic nanostructures allows the shifting of the light absorption in the visible range. Finally, we give an overview on the new strategies to increase the photocatalytic activity with new architectures and materials based on metal-oxides.

Keywords: photocatalysis, TiO₂, ZnO, heterostructures, plasmonic nanoparticles

1. Introduction

In the context of major environmental problems such as the lack of fresh water and the global planet warming, the most important expectations about photocatalysis are certainly coming from the perspective of energy storage and water/air depollution. Photocatalysis would allow

the direct transformation of solar energy into chemical energy for water splitting and hydrogen production [1], or water/air remediation of organic pollutants via redox reactions.

The implementation of depollution technologies in Europe has already been initiated. Numerous examples of self-cleaning and/or remediation cements, glass or paints are already commercialized by companies like Siplast (remediation membranes) [2], Calcia (self-cleaning and remediation cements) [3], Saint-Gobain (self-cleaning glass) [4], and Auro (Auro n°328, remediation paints) [5]. Among those commercial solutions a large debate on the real efficiency of those materials still exists [6]. As an example, the photocatalytic reduction of the concentration of NO_x in Leopold II tunnel in Brussels has been shown to be weak in spite of the use of photocatalytic cements. Indeed, the pollutants concentrations as well as the low power irradiation of the UV-visible light and the humidity conditions apparently impair the photocatalytic reaction. Concerning the water depollution or the hydrogen production, current installations do not exceed the scale of pilot demonstrators [7, 8].

A huge number of photocatalysts have already been reported in the literature and can be classified in the family of metal-oxides, metal-sulfides, metal-nitrides and also from metal free compounds like polymers or graphenes. In this chapter, our interest is principally focused on metal-oxides materials which are certainly the most studied when photocatalytic applications are concerned. In a non-exhaustive way, metal oxides like TiO_2 , ZnO , Fe_2O_3 , SnO_2 , ZrO_2 , MgO , GeO_2 , Sb_2O_3 , V_2O_5 , WO_3 , Cu_2O , In_2O_3 , Nb_2O_5 [9, 10], and perovskites are among the most investigated materials for the photocatalysis today. In the 70s, a photocatalytic activity was already known for TiO_2 or ZnO [11]. In the same decade, Fe_2O_3 , SnO_2 , ZrO_2 , MgO , GeO_2 , Sb_2O_3 , or V_2O_5 were also investigated as photocatalysts, but their activity were considered to be relatively weak compared to the one of TiO_2 [12, 13]. In the same years, Cu_2O was suspected to be involved in the photodegradation of polyethylene plastic [14]. First publications about organic dyes degradation by WO_3 were reported in 1993 [15], whereas In_2O_3 materials were shown to be active for the photodegradation of ethane in 1988 [16], and Nb_2O_5 to strongly increase TiO_2 activity toward the degradation of dichloro-benzene in 1994 [17].

Since the 70s, TiO_2 and in a lesser extent ZnO had continued to attract a particular interest in the research and industry communities. TiO_2 and ZnO present a high photocatalytic activity, good chemical stability, non- or low-toxicity, low cost, and more or less long term photostability. However, one of their important drawbacks is their lack of performances in the visible range of the solar spectrum.

The development of new photocatalysts appeared therefore to be a necessity to push forward the current photocatalytic performances. A lot of researches are currently conducted to find out new materials and/or improve the properties of the current ones. This chapter focuses on the enhancing strategies to boost the photocatalytic efficiency of the two most common photocatalysts, TiO_2 and ZnO .

Biocompatibility and/or durability properties of photocatalyst are rarely taken into consideration. We provide a prospective view of the pure photocatalytic performances or benefits of the cited materials, devices, or architectures. However, it is obvious that, to be selected as a

good candidate for commercial applications, a photocatalyst should not only demonstrate excellent photocatalytic activity but also needs to be biocompatible, low-cost, and durable.

Given that the photocatalysis is a surface based mechanism, one of the simplest ways to increase the activity is to increase the active surface area. Therefore, supported nanomaterials are obvious candidates of choice to reply to this challenge. The first section of this chapter describes nanotextured photocatalysts supported on porous template. In the second section, we focus the reader's attention on the band gap engineering that increase the separation of photo-generated carriers. The third section deals with the introduction of the plasmonic effect to shift in the visible range the light absorption properties of TiO₂ and ZnO photocatalysts. Finally, we propose an overview on the emerging new materials and concepts based on metal-oxides.

2. Nanostructured supported photocatalysts

In the earlier ages of photocatalysis, the experiments were conducted from bulk photocatalysts. The emergence of nanomaterials pushed in the late 80s by the development of characterization and visualization techniques stimulated a huge interest for those nanomaterials in the scientific community. Compared to bulk materials, nanomaterials exhibit a higher specific surface area. Two kinds of nanoscale photocatalysts can be distinguished: suspensions of nanostructures in solutions, or supported nanomaterials on appropriated templates. The main advantages of dispersed nanostructures are the simplicity of use and their low cost. Nevertheless, dispersed nanomaterials in solution tend to agglomerate, lowering their exposed specific surface area. Furthermore, a filtration step is needed to remove them from the solution. For this reason, a rising interest occurs on supported nanomaterials. In seek of always increasing the exposed specific surface area of nanotextured photocatalysts, their synthesis at the surface of porous support like membranes has been envisaged for water treatment [18, 19] or water splitting [20, 21]. Currently, membranes are mainly studied for the photocatalytic water treatment as they combine the double advantages of filtration, and photocatalytic degradation of water pollutants (hybrid filtration/photocatalytic membranes).

Stable photocatalytic membranes, can be obtained using inorganic membranes. The main advantages of inorganic membranes are their good chemical and thermal resistance. These allows the use of a wide panel of photocatalyst synthesis processes, like high temperature gas phase chemical vapor deposition (CVD), and hydrothermal growth followed by high temperature annealing. In addition, with those types of synthesis techniques many different photocatalytic structures of semiconductors can be achieved: nanoparticles, nanowires, nanorods, or nanofilms. Hong *et al.* [22] have pointed out the photocatalytic performances of Al₂O₃-ZrO₂ composite membrane coated with TiO₂ nanorods (**Figure 1a**) using a sol-gel process followed by an annealing step (510°C). The photocatalytic degradation curves of Methyl orange and Methylene blue (**Figure 1b**) clearly demonstrate an efficient photocatalytic activity of the elaborated membrane.

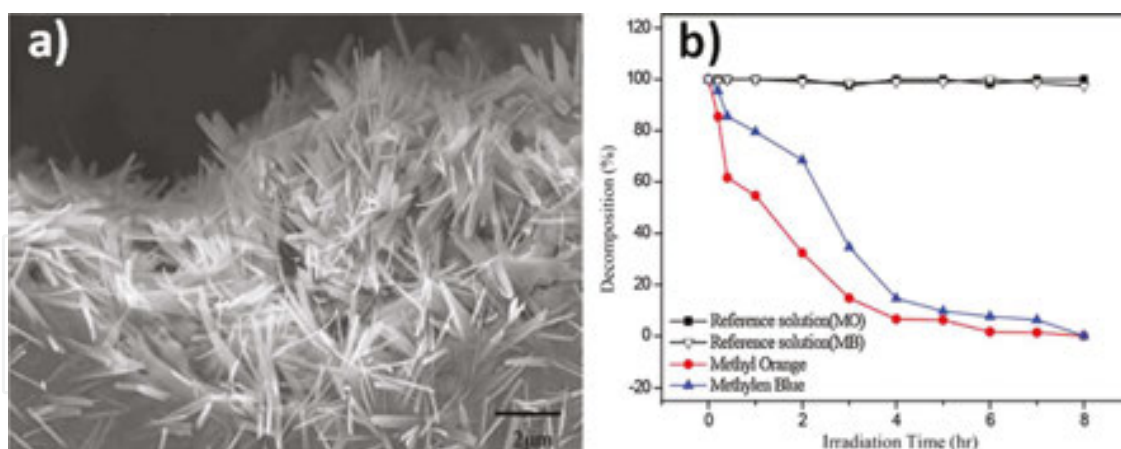


Figure 1. (a) Inside of a pore of a $\text{Al}_2\text{O}_3\text{-ZrO}_2$ composite membrane coated with TiO_2 nano-rods. (b) Photodegradation curves of Methylene blue and Methyl orange on a micro-channelled $\text{Al}_2\text{O}_3\text{-ZrO}_2$ composite membrane decorated with TiO_2 nano-rods. Picture reproduced from Hong *et al.* [22].

ZnO-based photocatalytic membranes can also be envisaged. Rogé [10] performed the growth of ZnO nano-wires inside glass fibers membrane with a solvothermal synthesis at low temperature (below 90°C). However, a better crystallinity of the ZnO, leading to better photocatalytic degradation properties can be reached after an annealing process around $200\text{--}300^\circ\text{C}$. The grown ZnO nano-wires on glass fibers are illustrated in **Figure 2**.

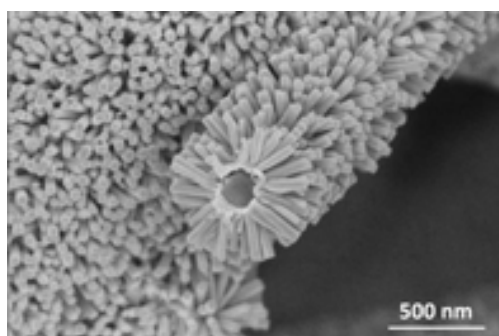


Figure 2. ZnO nanowires grown around glass fibers in a macro-porous glass fibers membrane.

When the pore size in membranes is lower than the micrometer scale, one technique is particularly adapted to the fabrication of photocatalytic porous membranes: atomic layer deposition (ALD). The ALD technique is indeed the most suitable gas phase technique for the growth of conformal metal-oxide nano-films inside porous structure. Rogé *et al.* [23] showed that ZnO nano-films grown by ALD between 150°C and 250°C exhibit good photocatalytic properties for the Methylene blue degradation. The authors highlighted that, for the same specific surface area, the ZnO realized by ALD are more active than other structures of ZnO grown in liquid or vapor phase. In another publication [24], the conformality of the ZnO deposited on nano-structured membranes of anodic aluminum oxide (AAO) has been also attested. **Figure 3** represents the cross-section of a ZnO film grown inside a 200 nm diameter AAO pore. We clearly notice the homogeneous film inside the porous structure.

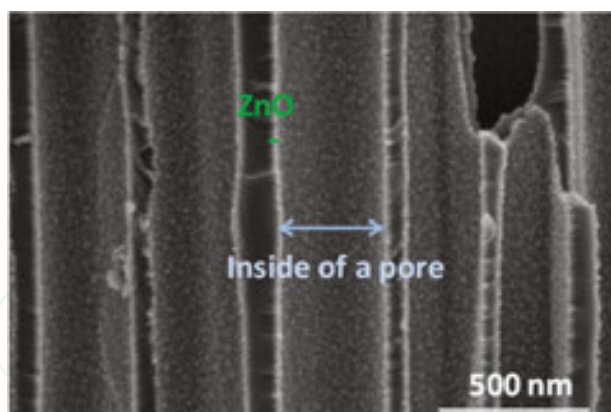


Figure 3. SEM picture of a ZnO nano-film grown in an anodic aluminum oxide membrane.

Similar results have been observed by Lee *et al.* [25]. They realized the synthesis of ZnO and TiO₂ nano-films inside bio-template membranes prepared from inner shell membranes of avian eggshells (**Figure 4**). They indicate that low temperature synthesis (100°C) of ZnO and TiO₂ leads to a ZnO-based material being more attractive for the photocatalytic activity, whereas at higher temperature synthesis (275°C), the TiO₂-based materials show more interesting bactericidal photocatalytic properties. Those results can be explained by the presence of a ZnO hexagonal crystalline structure at low temperature, being favorable to the electron/holes transport in the material. An amorphous structure, like the one of TiO₂ grown at low temperature, is less favorable for the charge carriers diffusion.

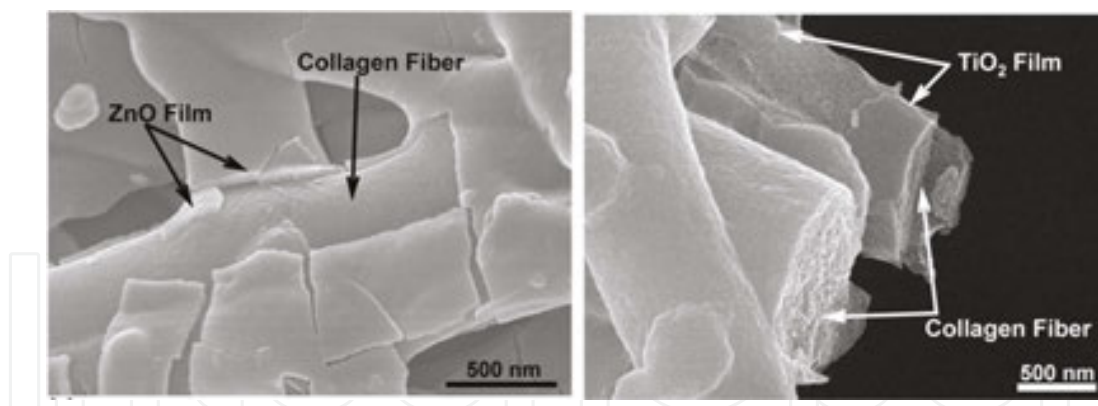


Figure 4. SEM picture of a composite membrane of collagen fibers and ZnO (on the left) and TiO₂ (on the right). Picture reproduced from Lee *et al.* [25].

Hybrid filtration/photocatalytic organic membranes can be synthesized by two different methods: deposition of the photocatalyst onto the membrane [26], or dispersion of the photocatalyst into the polymer [27]. The functionalization of organic membranes with TiO₂ nanoparticles can be performed by a dip coating [22] process using a TiO₂ precursor solution. This kind of membranes seems well adapted as they show improved hydrophilicity performance and photocatalytic properties due to the presence of the TiO₂ particles [28]. However, the immobilization of the TiO₂ nanoparticles is often not stable. Mansourpanah *et al.* [28] high-

lighted an important loss of TiO_2 nanoparticles from the membrane after a filtration process. To avoid this detrimental loss that may be prejudicial to the surrounding environment, a second approach consists in blending the photocatalyst in the polymer matrix. As an example, Rahimpour *et al.* [29] entrapped TiO_2 nano-particles in PVDF/SPES membranes using phase inversion induced by immersion precipitation process, as shown on the **Figure 5**.

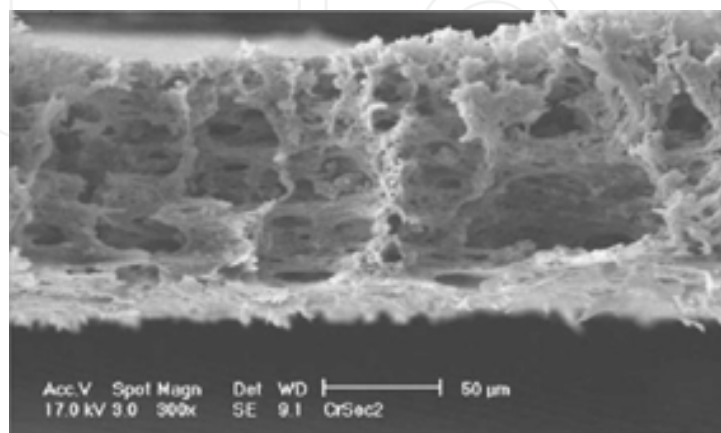


Figure 5. SEM picture of a PVDF/SPES membrane containing 4 wt% TiO_2 nano-particles. Picture reproduced from Rahimpour *et al.* [29].

The main drawback of the blended photocatalytic membranes is their limited photocatalytic performances compared to coated membranes, as the nano-particles are embedded in the polymeric matrix. As a consequence, an important part of photocatalysts does not contribute to the photodegradation mechanisms: either the UV light is trapped by the polymer [30], or either the electrons/holes photogenerated cannot migrate to the reactive surface in contact with pollutants species.

3. Improvement of the photocatalytic activity of photocatalysts by the fabrication of heterostructures

One of the limitations of the photocatalytic efficiency is the fast recombination of the photo-generated electron (e^-) and holes (h^+). Promoting the charge separation in photocatalysts is one strategy that has been proposed to increase the lifetime of the electron-hole pairs. The most common approaches include the development of (1) semiconductor/semiconductor heterostructures [31], (2) semiconductor/metal heterostructures [31, 32], (3) semiconductor/carbon heterostructure [31], or (4) the surface modification with electron or hole scavengers [33, 34].

Semiconductor/semiconductor heterostructures are defined when two semiconductors with different electronic band structures form a heterojunction. As illustrated in **Figure 6**, three types of heterojunctions can be distinguished based on the relative position of the conduction band and the valence band of the two semiconductors: the type-I or straddling gap, the type-II or staggered gap, and the type III or broken gap.

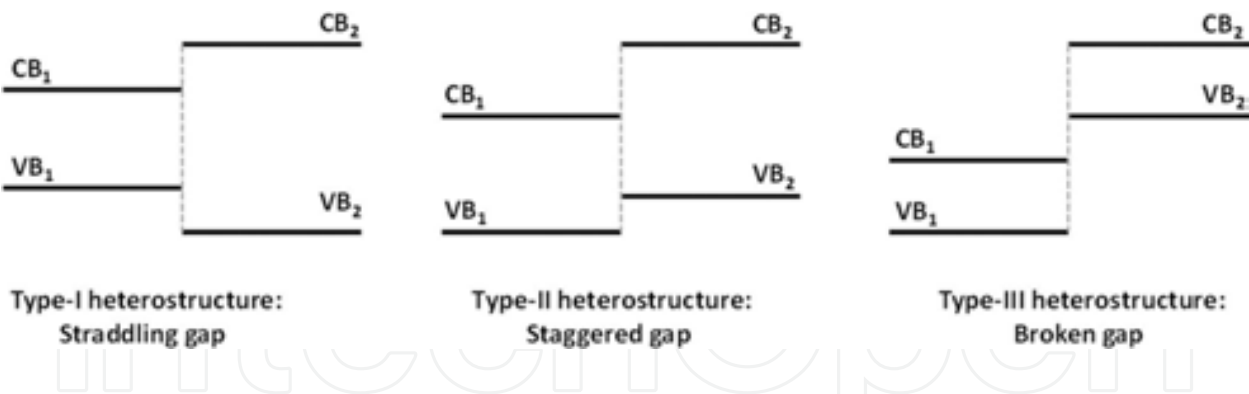


Figure 6. Representation of the three different heterostructures possible between two semi-conductors. CB₁ and VB₁ represent the conduction band and the valence band respectively of the semi-conductor 1. CB₂ and VB₂ represent the conduction band and the valence band respectively of the semi-conductor 2.

The type-II heterostructure is the most interesting one in photocatalysis as the energy gradient present at the interface allows the separation of the charge carriers on each part of the hetero-junction, as represented in **Figure 7**. For a typical ZnO/SnO₂ type-II heterostructure, the electrons photogenerated in the semiconductor with the highest conduction band energy (CB of ZnO) migrate in the conduction band of the semiconductor having the minimum conduction band energy (CB of SnO₂). Whereas the holes photogenerated in semiconductor with the lowest valence band energy (VB of SnO₂) migrate toward the valence band of the semiconductor having the maximum of valence band energy (VB of ZnO).

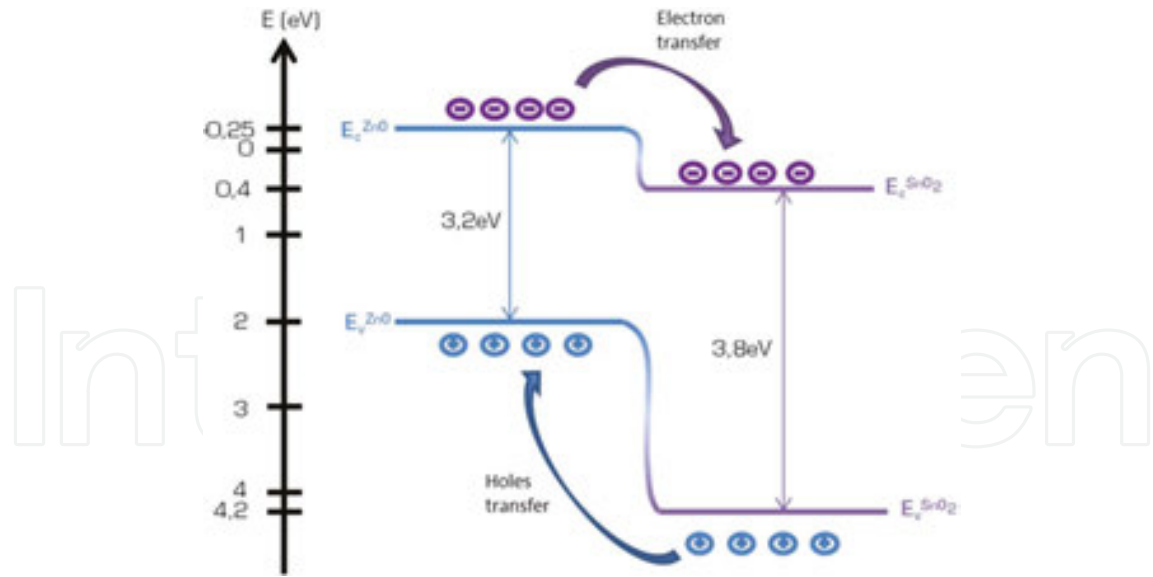


Figure 7. Representation of the type-II heterostructure present in a ZnO/SnO₂ heterostructure.

Rogé *et al.* [24] have characterized the bands alignment in the case of a ZnO nano-films/SnO₂ nano-particles heterostructure with XPS analysis. The valence band offset (VBO or ΔE_v), as well as the conduction band offset (CBO or ΔE_c) in the heterostructure are determined using the following equation:

$$\Delta E_v = \left(E_{Zn2p} - E_{v_{ZnO}} \right)_{ZnO\ bulk} - \left(E_{Sn3d} - E_{v_{SnO_2}} \right)_{SnO_2\ bulk} - \Delta E_{CL} \tag{1}$$

where E_{Zn2p} corresponds to the binding energy of the Zn2p peak in bulk ZnO, $E_{v_{ZnO}}$ to the valence band maximum of bulk ZnO, E_{Sn3d} to the binding energy of the Sn3d peak in bulk SnO₂ and $E_{v_{SnO_2}}$ to the valence band maximum in bulk SnO₂. The ΔE_{CL} term can be determined from:

$$\Delta E_{CL} = \left(E_{Zn2p} - E_{Sn3d} \right)_{heterostructure} \tag{2}$$

where E_{Zn2p} corresponds to the position of the Zn2p peak in the heterostructure of ZnO/SnO₂ and E_{Sn3d} to the position of the Sn3d peak in the heterostructure of ZnO/SnO₂.

The conduction band offset (ΔE_c) can be calculated using:

$$\Delta E_c = \Delta E_v + E_{g_{ZnO}} - E_{g_{SnO_2}} \tag{3}$$

where ΔE_v is the valence band offset previously calculated, $E_{g_{ZnO}}$ is the optical band gap of ZnO and $E_{g_{SnO_2}}$ is the optical band gap of SnO₂.

As a result, the band alignment at the ZnO/SnO₂ interface revealed a valence band offset around 0.67 eV and a conduction band offset around 0.24 eV, confirming the presence of a type-II heterostructure between those two materials.

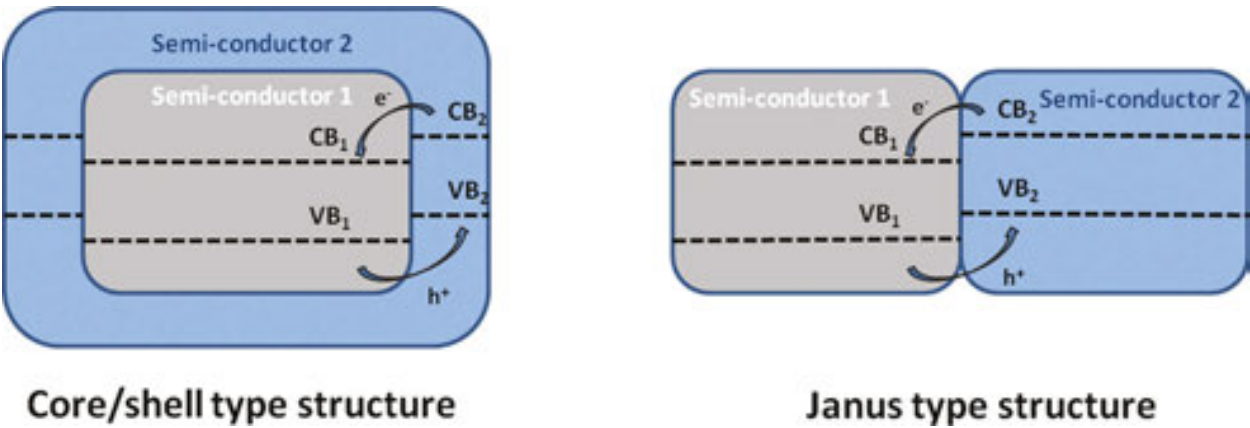


Figure 8. Representation of a core/shell (on the left) and a Janus type (on the right) heterostructure.

Two morphologies can be distinguished for the semiconductor/semiconductor heterostructures: the core/shell structure, and the Janus type structure (**Figure 8**). In a core/shell structure, one semiconductor is completely covered by the second one. Thus, only the charge carriers injected in the external material can undergo oxidative or reductive reactions at the surface.

In the Janus type structure, both materials are exposed to the environment. In this case, the two charge carriers e^- and h^+ are potentially available for oxidative or reductive reactions. Consequently, the Janus type morphology is the most studied in photocatalysis, as both e^- and h^+ can potentially be exploited. Therefore we focus on Janus type heterostructures.

Many different metal-oxide or metal-sulfide semiconductors are known to form a type-II heterostructure when coupled. Among them, ZnO- and TiO₂-based heterostructures are still strongly investigated: ZnO/SnO₂ [35–38], TiO₂/SnO₂ [39–41], TiO₂/ZnO [42–45], TiO₂/WO₃ [46], or ZnO/CuS [47]. ZnO and TiO₂ are two metal-oxides with similar properties. They both have a band gap around 3.2 eV, with light absorption properties in the near ultraviolet region. In addition, they have similar conduction and valence bands position. SnO₂ is a material with a much higher band gap, around 3.7 eV, absorbing far in the ultraviolet range, but the position of its conduction and valence bands relatively to the ZnO or TiO₂ ones makes it a suitable material for the development of a heterostructure with ZnO or TiO₂.

In the literature, different Janus type ZnO/SnO₂ and TiO₂/SnO₂ heterostructures have already been reported. Uddin *et al.* [36] have performed the synthesis of SnO₂/ZnO nano-particles forming a contact type heterostructure in liquid phase by precipitation/hydrothermal process. They have shown that the heterostructure allowed a two-time faster photocatalytic degradation of a methylene blue solution (10 mg.l⁻¹) under a UV light source (365 nm–125 W) compared to ZnO only. The same behavior has been observed by Cun *et al.* [37] with ZnO/SnO₂ nano-particles prepared also by a co-precipitation process in liquid phase. They highlighted a decolourization speed of a methyl orange solution 100% faster with ZnO/SnO₂ nanoparticles instead of ZnO nano-particles only. It is worth mentioning that the specific surface area of both materials (ZnO/SnO₂ and ZnO) used was in the same range and cannot explain such a difference in the photocatalytic performance. In their paper, De Mendonça *et al.* [41] synthesized TiO₂/SnO₂ nano-particles using two different liquid phase techniques: a hydrolytic sol-gel process and a polymeric process. The photocatalytic performance of those nano-particles, tested on Rhodamine B, was found to be 50% faster than commercial TiO₂ nano-particles.

ZnO/SnO₂ heterostructures composed of ZnO nanowires functionalized by SnO₂ particles can be synthesized using gas phase processes on flat surfaces or in porous membranes. Huang *et al.* [38] realized the growth of ZnO nanowires on silicon wafers, using a CVD process at high temperature (600°C) with Zn powder as zinc source and air as oxidant. The growth of SnO₂ nano-particles on top of the ZnO was performed also via a CVD process at high temperature (800°C) using SnO powder as tin source. The synthesized materials are presented on **Figure 9a**. The resulting photocatalytic performance showed a twofold improvement compared to ZnO only. Rogé *et al.* proposed an alternative method for the growth of ZnO nanowires covered by SnO₂ nano-particles at lower temperatures. ZnO nano-wires were synthesized by a solvothermal process below 90°C in a macro-porous glass fiber membrane (**Figure 9b**). A modified ALD process allowed the growth of SnO₂ nano-particles on the ZnO nano-wires at temperatures around 300°C.

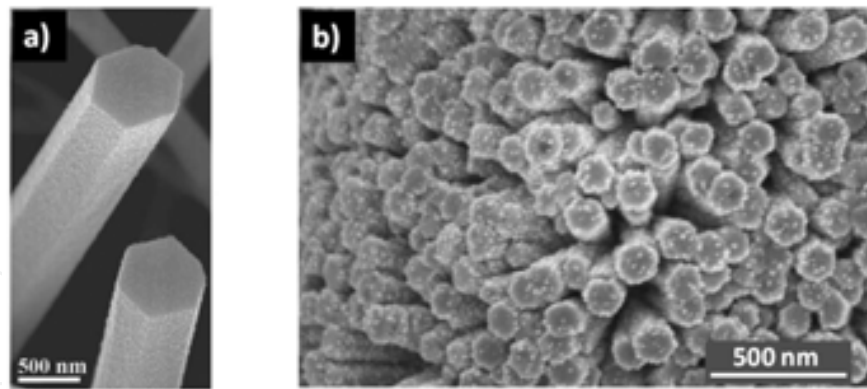


Figure 9. (a) SEM picture of ZnO/SnO₂ nano-wires/nano-particles grown by CVD. The picture was taken from Huang *et al.* [26]. (b) ZnO/SnO₂ nano-wires/nano-particles grown by hydrothermal/modified ALD processes.

Heterostructures of SnO₂/ZnO have been realized by Zhu *et al.* [48] using electrospun SnO₂ fibers that have been functionalized by ZnO nano-rods (**Figure 10a**) or nano-sheets (**Figure 10b**). The degradation rate of those ZnO decorated SnO₂ fibers is more than 100% faster than bare ZnO. If the authors did not analyze the SnO₂/ZnO heterostructure by XPS, they proved the charge separation in the ZnO/SnO₂ heterostructure by photo-current measurements. As depicted in **Figure 10c**, the photo-current produced by the ZnO/SnO₂ materials (named SZ-10/ZnO NRs and SZ-10/ZnO NSs) when illuminated under a simulated sunlight, shows a threefold intensity improvement compared to the bare ZnO.

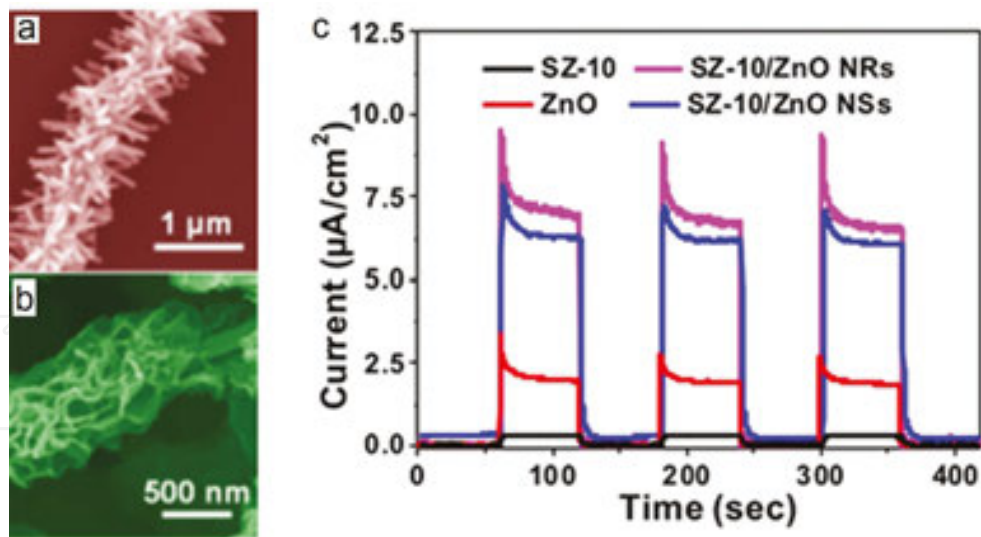


Figure 10. (a) SEM picture of a SnO₂ fiber decorated with ZnO nano-rods (SZ-10/ZnO NRs). (b) SEM picture of a SnO₂ fiber decorated with ZnO nano-sheets (SZ-10/ZnO NSs). (c) Photo-current responses of SZ-10/ZnO NRs, SZ-10/ZnO NSs and bare ZnO. Results copied from Zhu *et al.* [36].

This photo-current improvement results from the heterostructure formation which promotes an efficient separation of photo-excited electron-hole pairs and thus enhances the photocatalytic performance.

4. Plasmonics for visible light photocatalysis

4.1. How plasmonics work

Plasmonics deal with the core idea of a coherent oscillation of electrons in metals induced by the interaction of an incident electromagnetic radiation with metallic nanostructures.

A clear explanation of this phenomenon was suggested by Jones *et al.* [49]. The authors proposed an analogy with a mechanical oscillator. The displacement of a simple harmonic oscillator from equilibrium results into a continuous sinusoidal motion. An external periodical force applied to the system with an identical frequency (“in phase”) fulfills the resonance conditions and can therefore increase the amplitude of the harmonic oscillator. Similarly, in plasmonics, the incident electromagnetic light acts as the external force on the delocalized electrons (electrons cloud) of the conduction band and causes their enhanced displacement. Coulombic forces induced between the delocalized electrons cloud and the nucleus of the metal atoms are opposed to this displacement. The plasmon resonance corresponds to the conditions where the resultant of those two opposite phenomenon leads to the collective oscillation of the delocalized electrons (**Figure 11**).

In the case of metal nanoparticles, where the size is significantly lower than the light wavelength, the resulting collective oscillation of electrons is called *localized surface plasmon resonance (LSPR)*. The oscillation frequency mainly depends on the electrons properties, such as their density and effective mass, and also on the nanoparticles size, shape, and charge distribution [50, 51]. Among the numerous metals showing the LSPR, the noble metals are gaining popularity for their stability at the nanometer scale and the strong LSPR in the visible region of the sun spectrum.

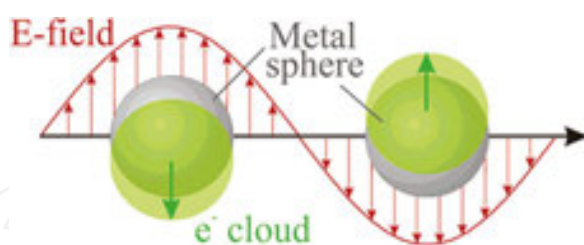


Figure 11. Schematic illustration of surface plasmon resonance. (reprinted with permission from ref. [50]).

The application of plasmonics in metal oxide photocatalysis is particularly interesting since the charge recombination, that reduces the degradation efficiency, and the narrowness of the absorbed sun irradiation (near UV range) is limited.

In the UV-visible range, nanoparticles act as small light concentrators and result in the increase of the electromagnetic field on the semiconductor surface due to the LSPR. Earlier publications, reporting on the enhancement of the photocatalytic activity using plasmonic nanoparticles coupled with semiconductor materials, focused on the ability of nanoparticles to promote the carriers separation. The proposed mechanism considers the interface between the photoca-

lytic semiconductor and the metallic nanoparticle as a Schottky barrier [52–57]. Under a visible range irradiation, the electrons could be injected from the photo-excited metal to the semiconductor (**Figure 12a**). As an example described in **Figure 12a**, this electron transfer modifies the gold into an oxidized state. According to a mechanism proposed by Tian and Tatsuma [54], the oxidized gold could be immediately reduced by an electron donor present in the solution. Furube *et al.* [55] demonstrate in 2007, by femtosecond IR probe, that this electron injection occurs within few hundreds femtoseconds.

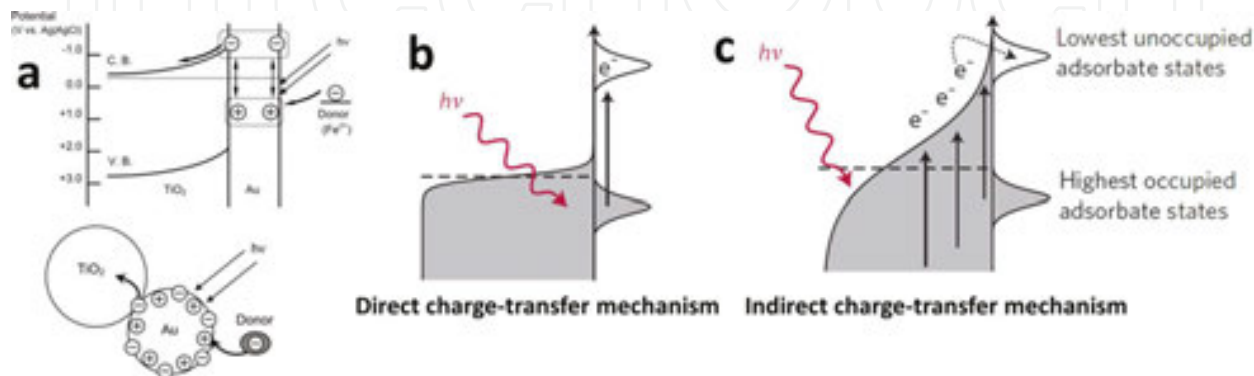


Figure 12. (a, b) Possible mechanism of charge separation (direct charge transfer mechanism). (c) Indirect charge-transfer mechanism (reprinted with permission from refs. [54, 58]).

However, the complete understanding of mechanisms leading to this enhancement is not fully achieved. The mechanism related to the *direct charge injection* found an important support through theoretical and experimental investigations [58–60]. Linic *et al.* consider that the direct electron injection occurs via the direct excitation of an electron to an unoccupied adsorbate state of the semiconductor without the formation of an excited electron distribution in the metal (**Figure 12a** and **b**). However, the authors propose to take into consideration another plausible mechanism – *indirect charge transfer* (**Figure 12c**). The indirect charge-transfer mechanism considers that energetic charge-carriers are formed under the influence of the electric field. The excited charge-carriers interact with orbitals close to Fermi level and the plasmon relaxation results in an electron distribution above the metal Fermi level [58, 61].

Another important fact to be taken into account is the effect of local heating on the plasmonic nanoparticles. This phenomenon happens because of the local electromagnetic field induced by the plasmonic phenomena. This effect has already been used in photothermal therapy in medicine [62] and in photoassisted synthesis [63, 64]. In this evidence, Fasciani and co-workers [65] have estimated that the temperature raising on the surface of a gold nanoparticle exposed to a laser pulse (8 ns at 532 nm, 50 mJ/pulse) could achieve $500 \pm 100^\circ\text{C}$.

The literature overview does not provide a clear mechanism of how exactly LSPR effect activates the wide band gap semiconductor in the visible range. However, the main adopted mechanism is the direct carriers transfer from the excited metal nanoparticle into the semiconductor [51, 52, 54, 55, 58, 66–68].

Various combinations of assembly of the conventional photocatalysts material (TiO₂, ZnO, CeO, Fe₂O₃, CdS, etc.) with plasmonic nanoparticles, typically silver, gold, platinum, or mixed alloys are currently reflected in the literature [69].

4.2. Architecture of plasmonic systems

The decoration of the photocatalytic surface by plasmonic nanoparticles shows an enhancement of the photocatalytic activity. Yet, the coverage by more than 15% of metal nanoparticles inhibits the plasmonic enhancement by the reduction of the specific surface area of the semiconductor [57, 70, 71].

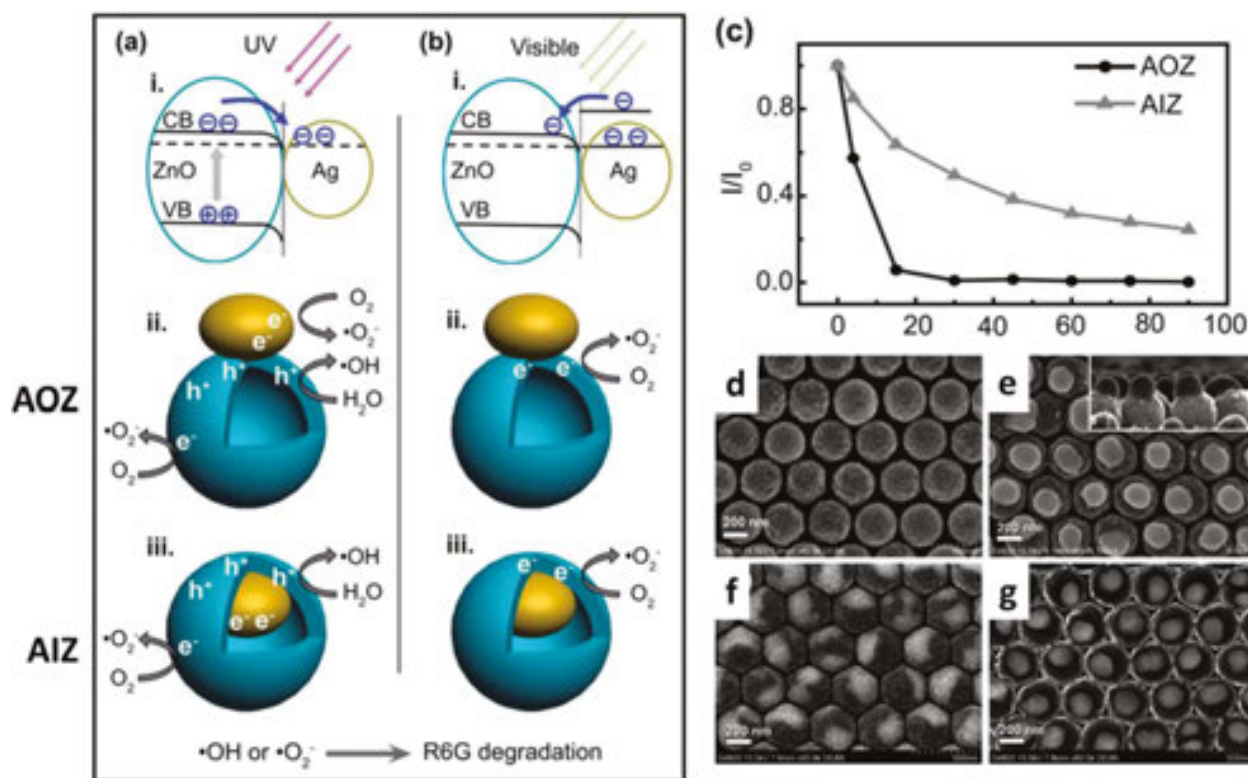


Figure 13. Energy band gap and photocatalytic mechanisms of asymmetric arrays Ag on top of ZnO nanospheres (AOZ) and Ag inside ZnO (AIZ) under (a) UV light and (b) visible light. (c) Photocatalytic degradation plot; SEM images for (d) ZnO nanospheres, (e) AOZ arrays, (f) top view AIZ arrays, and (g) AIZ arrays internal structure (reprinted with permission from ref. [72]).

An important number of publications investigate the possible architectures which would allow getting maximum LSPR effect without depleting the photocatalytic activity. Zang *et al.* [72] have demonstrated that the architecture plays an important role. The authors realized two different asymmetric composite arrays of hollow ZnO nanospheres and silver nanoparticles placed on top and inside ZnO spheres (Figure 13). ZnO spheres were supported on Silicon substrates. In both cases the local enhancement of the field has a double impact: improvement of light adsorption on the semiconductor material and charge separation. Comparing the photocatalytic activity of both configurations, placing a nanoparticle inside a nanosphere

reduces the degradation rate. The comparison of asymmetric assembly architectures was also demonstrated by Seh *et al.* [73] using different types of Au-TiO₂ nanostructures assembly, such as Janus (**Figure 14a**) and core-shell (**Figure 14b**).

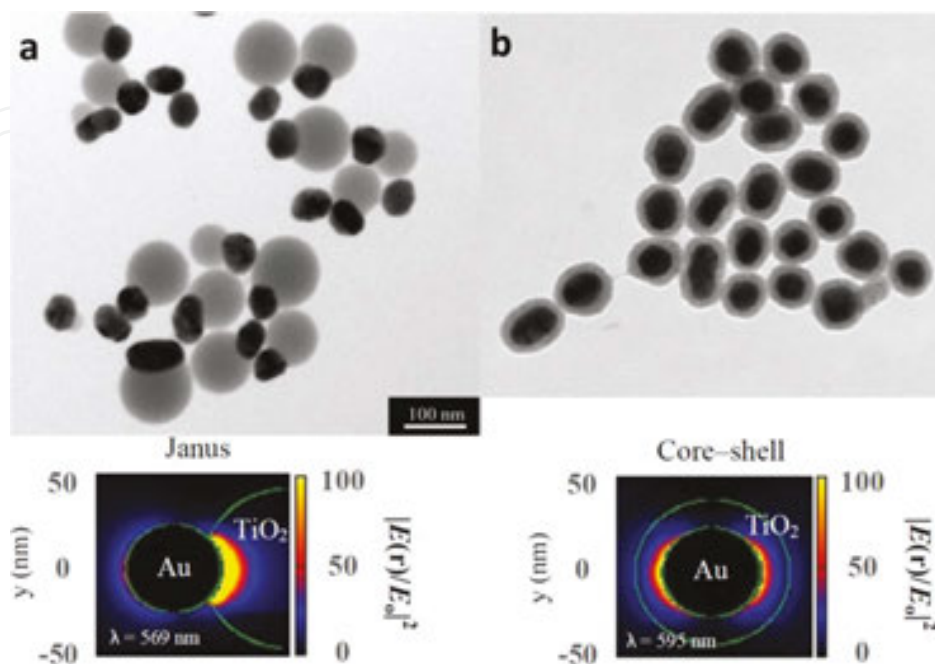


Figure 14. Illustration for Janus (a) and core-shell (b) Au 50 nm-TiO₂ nanostructures and their plasmonic near-field maps obtained by DDA simulation (reprinted with permission from ref. [73]).

Discrete dipole approximation (DDA) calculations and experimental investigations on both type of TiO₂ assembly with 50 nm gold particles showed an enhancement of the electric near-field intensity due to the high refractive index of TiO₂ on the materials interface. In Janus structures the plasmonic near-field is localized on one side of gold nanoparticle (non-symmetric distribution) whereas in core-shell configuration, it provides a symmetric distribution. However, the power of absorbed light on non-symmetric Janus nanostructures was 1.75 times larger than the one of core-shell. It results in an increase of the efficiency of photocatalytic hydrogen production by 1.7 times compared to the core/shell structure and confirms that Janus configuration has more benefits for the photocatalytic enhancement. Actually, in Janus type assembly, the plasmonic near field is localized close to the Au-TiO₂ interface and the carrier's generation occurs closer to the TiO₂ surface. Therefore, the carrier's recombination is decreased and the carrier injection into the semiconductor is improved. These results confirm that plasmonic nanoparticles on top of the semiconductor material, instead of inside, result in significant improvement of the photocatalytic activity. A different type of core-shell structures was designed by Eom and co-workers [74]. A periodic array of open core-shell Ag-TiO₂ nanostructures was realized using nanoimprint lithography (NIL) and UV-sensitive resin. The silver nanowires were formed by thermal evaporation from Ag-target on the patterned substrate and following TiO₂ coating was electrodeposited. This type of core-shell structures also demonstrated an important enhancement of the photocatalytic activity in UV and visible

ranges. The degradation of Methylene blue under visible light evidences 9 times improvement of the photocatalytic efficiency when compared to simple TiO₂ film.

Studies investigate low cost metals for plasmonic applications such as aluminum. According to finite-difference time domain (FDTD) simulation Al/CdS core-shell system realized by Duan and Xuan. [75], demonstrate a significant enhancement of optical absorption in the visible range. Authors also conclude on the importance of the core/shell ratio (radius ratio) which should be equal to 30/40 nm to achieve the strongest absorption.

Recently, Hao and co-authors [76] reported the enhancement of light absorption on Al/TiO₂ structures due to the LSPR effect on aluminum nanostructures. The aluminum nano-void arrays were fabricated by the anodizing process. Typically, the fabrication process of nano-voids includes two steps: an anodization followed by a chemical etching of the grown alumina. The UV-visible spectra of nano-voids demonstrate the presence of the SPR which could be tuned by the size of the aluminum nano-voids. However, the response was restricted to the UV range only (**Figure 15**).

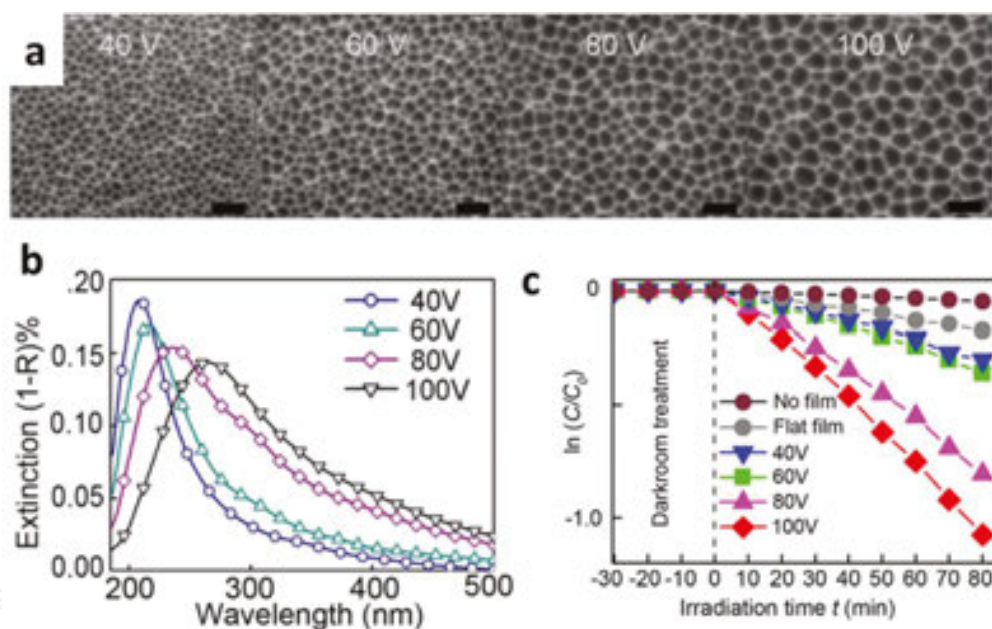


Figure 15. (a) SEM images of the aluminum foils with nano-void arrays (scale bar being 500 nm). (b) UV-visible spectra of nano-voids. (c) Photocatalytic degradation of Rhodamine B under UV-visible irradiation (reprinted with permission from ref. [76]).

Although aluminum nano-voids show the plasmonic enhancement of the light absorption, the samples with TiO₂ coating do not manifest significant improvement of the photocatalytic activity in the visible range. However, an increase of the degradation rate in the UV range could still be observed by plasmonic effect [76].

Another interesting approach that is claimed to improve the light absorption in the semiconductors for photovoltaic or photocatalytic application is the assembly of plasmonic nanoparticles into a periodic structure [77]. The well-controlled nanoparticles deposition with precise

size and spacing control can induce advantageous optical effect for the light management. For instance, placing nanoparticles in a close proximity (1 nm) has an important effect on their scattering performance and their near-field due to the local coupling effect [78]. If this inter-particles distance could be well controlled, that would offer the possibility of tailoring the light scattering and the light absorption on the semiconductor (**Figure 16**) [77]. This promising approach attracts a strong interest for the photovoltaic application but could be also successfully implemented for the photocatalytic devices.

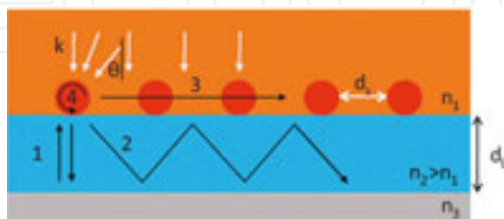


Figure 16. Representation of four common modes for increasing of light absorption: Fabry–Perot resonance (1), guided resonance (2), grating coupling (3), and Whispering gallery modes (4) (reprinted with permission from ref. [77]).

5. Overview on the emerging new materials and concepts

5.1. New materials to design photocatalysts

New emerging materials, strategies, and/or architectures based on metal-oxides allows to push forward the photocatalytic performances. Ideally, those materials and systems should be durable and eco-friendly. As already largely well described in the literature [79–82], several steps need to take place in a photocatalytic phenomenon: the excitation of the photocatalyst that leads to electron-hole pair creation, their migration toward the surface, the adsorption of the reactant, and finally the redox reactions. The enhancement of the photocatalytic efficiency depends on how the photocatalytic materials or architectures can promote at least one of these parameters without deteriorating the others. As the abundance of ideas in the scientific community is high, we could certainly not claim to be exhaustive, but we believe that the reader will find here the most important matter to have a fairly large view on what is currently set about the improvement of the efficiency of photocatalytic systems.

5.1.1. Binary oxides

Few binary metal oxides have been reported to be active in water splitting [83]. Cerium oxide is a fairly recent binary metal oxide material that has been shown to have a water splitting activity when doped by Strontium [84] or more recently as oriented hexagonal nanorods on Titanium substrates with a Na_2S - Na_2SO_3 sacrificial agent [85]. This last material had also been successfully used for the degradation of pollutants. Tang *et al.* [86] demonstrated a photocatalytic degradation of aromatic benzenes by CeO_2 nanotubes in air. The cerium oxides

nanomaterials were grown from hydrothermal synthesis of Ce(OH)CO₃ precursors with alkali solution in an aqueous phase.

In a recent review, Miseki *et al.* [83] reported others recent materials that present a water splitting activity : binary oxides like Ga₂O₃ doped with Zinc and coupled to a cocatalysts, mesostructured crystalline Ta₂O₅ with a 3% cocatalyst of NiO_x and TiS₂.

5.1.2. Ternary and quaternary metal oxides

Most of metal oxides that exhibit an activity in water splitting are ternary or quaternary metal oxides. Boosted by the societal interest of the hydrogen fuel cell production, most of the novel photocatalytic materials have been applied to water splitting [9]. Among them, perovskite materials occupy a place of choice. Recently, metal halide perovskites for photovoltaics have emerged as a contender of the leading photovoltaic materials. Indeed their power to conversion efficiency had grown from 3% to 20% in four years [87]. Those impressive performances raise interests to scrutinize if such performance could be reached in the photocatalytic field.

Perovskite minerals were originally associated to CaTiO₃ in homage to Lev Perowski (1792–1856) but are now more generally designating materials with the general chemical formula ABX₃ (where A is a rare or alkaline earth metal, B is a transition metal, and X the oxygen generally) and the kind of crystallographic structure illustrated in **Figure 17**.

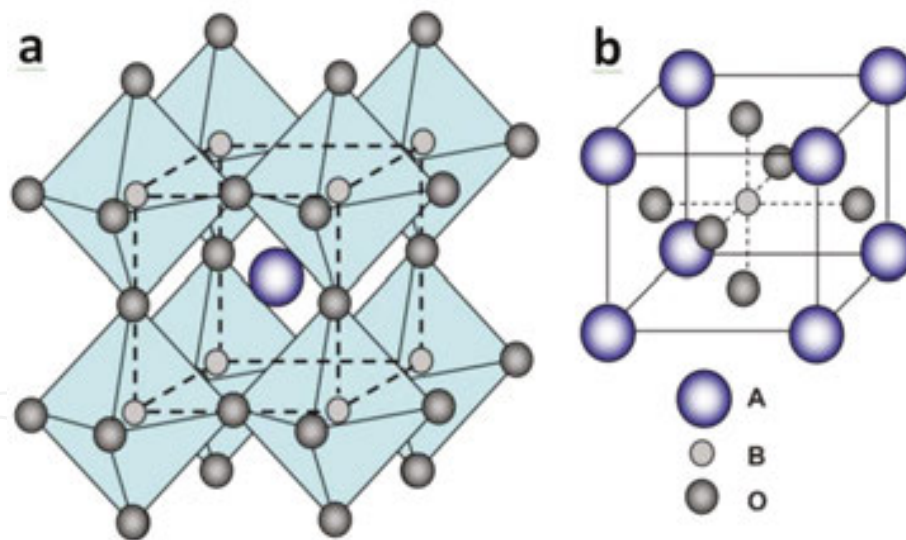


Figure 17. Crystallographic structure of a perovskite lattice. (a) BO₆ octahedral view with A site surrounded by 12 coordinated interstices. (b) Cubic lattice with B-site cation at the center of the cell (reprinted with permission from ref. [88]).

The most studied compounds revolve around the periodical elements Ta, Ti, Nb, Sn, V, Fe as B sites which found photocatalytic applications related to both hydrogen fuel production or degradation of pollutants. Some interesting results have already been reported: Grewe *et al.* [89] for example recently showed the simple hydrothermal synthesis of NaTaO₃ nanoparticles leading to the hydrogen production rate of 94 μmol/h. Yin *et al.* [90] prepared also via hydro-

thermal synthesis octahedral shaped PbTiO_3 nanocrystals with well define (111) facets that exhibit interesting performances related to the degradation of Methylene blue. These results have never been reported in conventional perovskite systems (100% degradation of Methylene blue 10^{-5} M after 35 min of irradiation). Perovskite materials present several advantages reviewed by Tanaka and Misono [91]: a large variety of compositions and chemical elements can be used while keeping the basic structure and their valency, stoichiometry, and vacancy concentration can be varied widely. Finally, a lot of information on their physical and solid state chemical properties has been accumulated. Strategies to boost their photocatalytic performance consist frequently in A, B, or X site doping (N_3^- doping of oxygen sites to oxynitrides for example) but also in the development of new synthesis methods or the improvement of the current ones [92].

Jingshan *et al.* [93] unveiled the first water-splitting cell with 12.3% efficiency based on $\text{CH}_3\text{NH}_3\text{PbI}_3$ (see **Figure 18**) and opened the route to the use of such metal halide perovskites in photocatalysis.

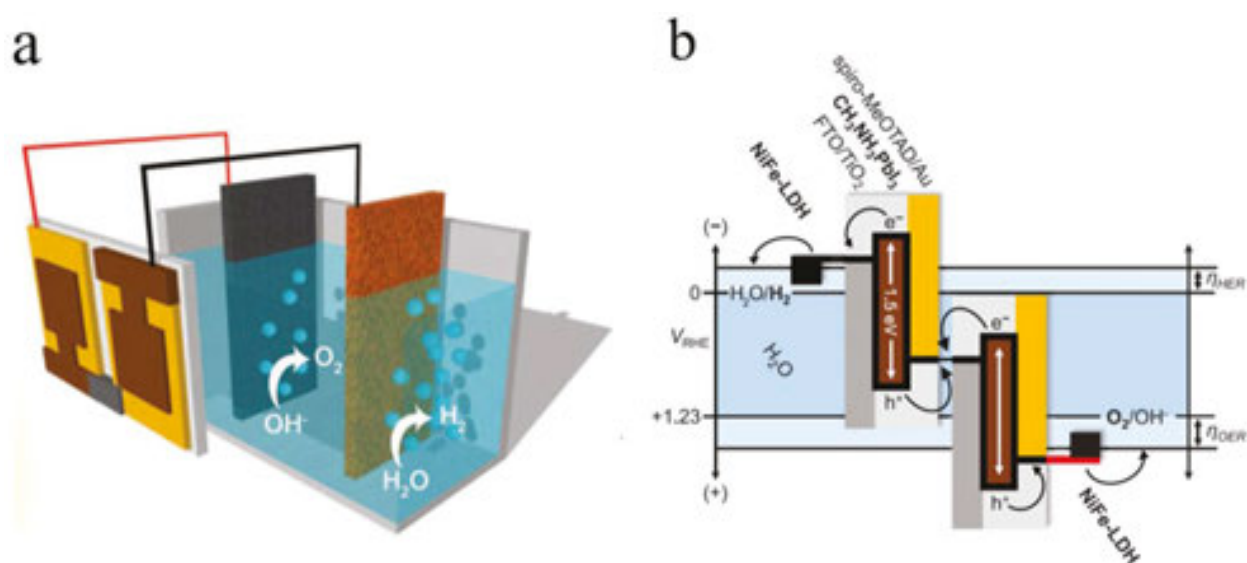


Figure 18. Jinshan water photolysis device. (a) 3D representation. (b) Schematic including the materials used for the cocatalysts and the light sensitive parts as well as the energy levels of water oxidation and reduction (reprinted with permission from ref. [93]).

Pyrochlore metal oxides with the general chemical formula $\text{A}_2\text{B}_2\text{O}_7$ are certainly less known than perovskite but are also investigated [82]. The angle B-O-B close to 180° in those structures is reported to facilitate the migration of the electron-hole pairs and is a good illustration of how the crystallographic structure of a photocatalyst can impact the photocatalytic degradation processes. Vanadium derived compounds based on the general chemical formula $\text{M}_3\text{V}_2\text{O}_8$ were synthesized in 2005 and more recently MVO_4 ones were reported to be active in the degradation of dye waste water under visible light irradiation [94]. Molybdenum or Tungsten derived compounds like $\text{Bi}_2\text{Mo}_2\text{O}_9$, ZrMo_2O_8 , NiMoO_4 , Bi_2WO_6 , and Bi_2WO_6 are also

known as photocatalysts applied to the degradation of pollutants (Methyl Orange, Rhodamine B, Malachite green).

Finally the layered perovskites, for which photocatalytic activity was already reported in the 90s, continue to be under investigation and give promising results [95]. Aurivillius Layered Perovskites, Bi_{5-x}La_xTi₃FeO₁₅ (x = 1, 2) were demonstrated to be particularly active for the degradation of Rhodamine B (RhB) under sun-light irradiation in mild acidic medium. Supramolecular structures like MOFs (metal organic frameworks) or polyoxometallates have also recently been reviewed as they can exhibit some interesting photocatalytic properties [9].

Generally speaking, the chemical construction of a potentially efficient photocatalyst for water splitting draws from the Mendeleev table metal cations with a d⁰ or d¹⁰ electronic configuration. They are involved in the construction of the crystal and energy structure. Alkali, alkaline earth, and some lanthanide ions do not play a role directly in the band formation but simply contribute to the construction of the crystal structure. **Figure 19** summarizes the key chemical elements that can play a role to design new photocatalytic materials.


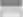


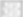


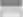


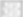


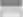


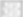

| | | | | | | | | | | | | | | | | | | | | | | | | | | | | | | | | | | | | | | | |
|--|---|-----------------------|---|----|----|----|----|----|----|----|----|----|----|----|----|----|----|----|---|----------------------|---|----|---|-----------------------|----|---|-------------|-----|---|----|---|------|---|--|------------------------------------|-----|---|--|----------------------------|
| 1 | 2 | 3 | 4 | 5 | 6 | 7 | 8 | 9 | 10 | 11 | 12 | 13 | 14 | 15 | 16 | 17 | 18 | | | | | | | | | | | | | | | | | | | | | | |
| H | | | | | | | | | | | | | | | | | He | | | | | | | | | | | | | | | | | | | | | | |
| Li | Be | | | | | | | | | | | B | C | N | O | F | Ne | | | | | | | | | | | | | | | | | | | | | | |
| Na | Mg | | | | | | | | | | | Al | Si | P | S | Cl | Ar | | | | | | | | | | | | | | | | | | | | | | |
| K | Ca | Sc | Ti | V | Cr | Mn | Fe | Co | Ni | Cu | Zn | Ga | Ge | As | Se | Br | Kr | | | | | | | | | | | | | | | | | | | | | | |
| Rb | Sr | Y | Zr | Nb | Mo | Tc | Ru | Rh | Pd | Ag | Cd | In | Sn | Sb | Te | I | Xe | | | | | | | | | | | | | | | | | | | | | | |
| Cs | Ba | La | Hf | Ta | W | Re | Os | Ir | Pt | Au | Hg | Tl | Pb | Bi | Po | At | Rn | | | | | | | | | | | | | | | | | | | | | | |
| <table border="1"> <tr> <td>Ce</td><td>Pr</td><td>Nd</td><td>Pm</td><td>Sm</td><td>Eu</td><td>Gd</td><td>Tb</td><td>Dy</td><td>Ho</td><td>Er</td><td>Tm</td><td>Yb</td><td>Lu</td> </tr> </table> | | | | | | | | | | | | | | | | | | Ce | Pr | Nd | Pm | Sm | Eu | Gd | Tb | Dy | Ho | Er | Tm | Yb | Lu | | | | | | | | |
| Ce | Pr | Nd | Pm | Sm | Eu | Gd | Tb | Dy | Ho | Er | Tm | Yb | Lu | | | | | | | | | | | | | | | | | | | | | | | | | | |
| <table> <tr> <td>i)</td> <td></td> <td>: d⁰ ion</td> <td rowspan="3">} to construct crystal structure and energy structure</td> </tr> <tr> <td></td> <td></td> <td>: d¹⁰ ion</td> </tr> <tr> <td></td> <td></td> <td>: Non-metal</td> </tr> <tr> <td>ii)</td> <td></td> <td></td> <td>to construct crystal structure but not energy structure</td> </tr> <tr> <td>iii)</td> <td></td> <td></td> <td>to form impurity levels as dopants</td> </tr> <tr> <td>iv)</td> <td></td> <td></td> <td>to be used for cocatalysts</td> </tr> </table> | | | | | | | | | | | | | | | | | | i) |  | : d ⁰ ion | } to construct crystal structure and energy structure | |  | : d ¹⁰ ion | |  | : Non-metal | ii) |  | | to construct crystal structure but not energy structure | iii) |  | | to form impurity levels as dopants | iv) |  | | to be used for cocatalysts |
| i) |  | : d ⁰ ion | } to construct crystal structure and energy structure | | | | | | | | | | | | | | | | | | | | | | | | | | | | | | | | | | | | |
| |  | : d ¹⁰ ion | | | | | | | | | | | | | | | | | | | | | | | | | | | | | | | | | | | | | |
| |  | : Non-metal | | | | | | | | | | | | | | | | | | | | | | | | | | | | | | | | | | | | | |
| ii) |  | | to construct crystal structure but not energy structure | | | | | | | | | | | | | | | | | | | | | | | | | | | | | | | | | | | | |
| iii) |  | | to form impurity levels as dopants | | | | | | | | | | | | | | | | | | | | | | | | | | | | | | | | | | | | |
| iv) |  | | to be used for cocatalysts | | | | | | | | | | | | | | | | | | | | | | | | | | | | | | | | | | | | |

Figure 19. Chemical elements from the Mendeleev table to construct a photocatalyst (reprinted with permission from ref. [83]).

5.2. New strategies to design photocatalysts

The example about new halides perovskites illustrates how photovoltaics research can inspire the one conducted in photocatalysis. The recent 3D TiO₂ anatase nanostructures based solar cell developed by Wu *et al.* [96] which reach a power conversion efficiency of 9.09% (to be compared to the 5% one for the same material as simple nanowires of same thickness), could be an interesting candidate for photocatalytic applications (**Figure 20**). In this work, the authors start from TiO₂ anatase nanowires grown by hydrothermal methods. Acid thermal reaction was then used to produce on the nanowires, TiO₂ nanosheets on which nanorods were finally grown by a last hydrothermal reaction step.

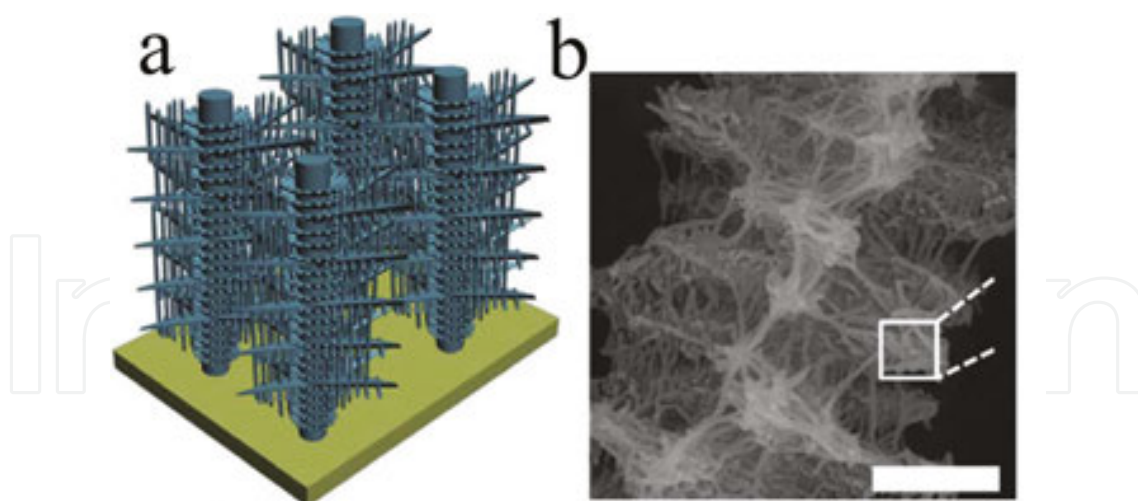


Figure 20. TiO₂ hyperbranched nanostructures. (a) 3D representation, (b) SEM image of the interlaced nanowires, nanosheets, and nanorods (scale bar: 500 nm) (reprinted with permission from ref. [96]).

Li *et al.* [97] recently reported the fabrication of TiO₂ nanoparticles with sub-10 nm dimensions that exhibit visible light driven photocatalytic hydrogen production. With a 1% platinum cocatalyst deposited on nanoparticles, the photocatalytic hydrogen production performance was 932 $\mu\text{mol}\cdot\text{h}^{-1}\cdot\text{g}^{-1}$ under visible light ($400\text{ nm} < \lambda < 780\text{ nm}$).

Ultrathin 2D nanomaterials, which are comparable to graphene type materials with sheet-like structures find more and more applications including photocatalysis [98]. Recently Zhou *et al.* [99] successfully separated 2D ultrathin Bi₂WO₆ monolayers from the same nanocrystal and showed excellent photodegradation of Rhodamine B under visible light with a separation of holes and electrons on two different active sites located at two different layers. An excellent hydrogen production activity under visible light is also reported for this new kind of horizontally designed heterostructures. Similarly, 2D nanosheets of the layered perovskite, Ba₅Nb₄O₁₅, were synthesized by a hydrothermal route. The nanosheets showed much enhanced photocatalytic activity compared to thick nanosheets for the production of H₂ from water splitting under UV light illumination. The enhanced activity is predominantly attributed to the larger surface area, higher optical absorption, and charge separation ability of the 2D nanosheet.

6. Conclusion

In this chapter, we highlighted different strategies to improve the photocatalytic performance of TiO₂- and ZnO-based nanomaterials. We pointed out the benefits of photocatalytic filtration membranes functionalized with TiO₂ and ZnO nanostructures. Due to their high specific surface area and their filtration properties, photocatalytic membranes allow the filtration and the degradation of organic pollutants. In some cases, especially after dip coating synthesis processes, the stability of nanomaterials at the surface of the membranes is not sufficient, resulting in a leakage of the photocatalyst in the environment. In the second section, we

discussed the strategies to improve the photocatalytic properties of ZnO and TiO₂ photocatalysts by engineering heterostructures with other metal-oxides, like SnO₂. We showed that TiO₂/SnO₂ and ZnO/SnO₂ type-II heterostructures lead to efficient charge carriers (e⁻ and h⁺) separation toward each electrode of the heterojunction, resulting in a longer lifetime of both carriers. As a result, improved photocatalytic performance is observed. In the third section, we present a strategy to activate TiO₂ and ZnO photocatalysts in the visible range of the sunlight spectrum, using the plasmonic effect in metal-oxides materials decorated with metallic nanoparticles. We describe different mechanisms explaining the impact of the plasmonic effect on the photocatalytic activity in the visible range. In a last section, new promising nanomaterials and nanoarchitectures based on binary, ternary, and quaternary metal-oxides have been reviewed.

Author details

Olga M. Ishchenko, Vincent Rogé, Guillaume Lamblin* and Damien Lenoble

*Address all correspondence to: Guillaume.lamblin@list.lu

Luxemburg Institute of Science and Technology, Esch-Sur-Alzette, Luxembourg

References

- [1] Pasternak S, Paz Y. On the similarity and dissimilarity between photocatalytic water splitting and photocatalytic degradation of pollutants. *ChemPhysChem*. 2013;14(10): 2059–70.
- [2] Siplast. Available from: <http://www.siplast.fr/profil/maitres-ouvrage-maitres-oeuvre/nox-activ-video>.
- [3] Calcia. Available from: <http://fr.i-nova.net/fr/content?articleId=198660>.
- [4] Saint-Gobain. Available from: <http://fr.saint-gobain-glass.com/product/937/sgg-biocleane>.
- [5] Auro. Available from: http://www.auro.fr/produits_3.php?sub_id=26.
- [6] Gallus M, Akylas V, Barmpas F, Beeldens A, Boonen E, Boréave A, et al. Photocatalytic de-pollution in the Leopold II tunnel in Brussels: NO_x abatement results. *Build Environ*. 2015;84(2):125–33.
- [7] Guo L. Advances in solar hydrogen technologies. *SPIE Newsroom*. 2011;10–2. Available from: <http://www.spie.org/x48082.xml>.
- [8] Sowarla GmbH. Available from: <http://www.sowarla.de/demonstration-plant.html>.

- [9] Hernández-Alonso MD, Fresno F, Suárez S, Coronado JM. Development of alternative photocatalysts to TiO₂: Challenges and opportunities. *Energy Environ Sci.* 2009;2(12): 1231.
- [10] Rogé V., PhD Thesis, Etude, Fabrication et Caractérisation de nanostructures catalytiques de type ZnO/SnO₂ intégrées à des membranes modèles pour la dépollution de l'eau. Université de Strasbourg. 2015.
- [11] Bickley RI. Photo-induced reactivity at oxide surfaces. M W Roberts, J M Thomas editors. *Chemical Physics of Solid and their Surfaces*. Royal Society of Chemistry 1977, Vol. 7, pp. 118–56.
- [12] Formenti M, Juillet F, Meriaudeau P, Teichner SJ, Vergnon P. Preparation in a hydrogen-oxygen flame of ultrafine metal oxide particles. *Aerosols Atmos Chem.* 1972;1:79-89.
- [13] Francois J, Stanislas Teichner MF. Process for the photocatalytic oxidation of hydrocarbons into aldehydes and ketones. United State Patent n°3781194, 1973. pp. 1–7.
- [14] Belokoneva GI, Demchenko SS, Red'ko LA, Kachan AA, Chervyatsova LL. Effect of some fillers on the photo- and thermal decomposition of polyethylene. *Plast Massy.* 1975;(1):57–8.
- [15] Bedja I, Hotchandani S, Kamat PV. Photoelectrochemistry of quantized WO₃ colloids: Electron storage electrochromic and photoelectrochromic effects. *J Phys Chem.* 1993;97:11064–70.
- [16] Sato S. Photocatalytic activities of indium oxide powder prepared from indium hydroxide. *J Photochem Photobiol A Chem.* 1988;45(3):361–7.
- [17] Cui H, Dwight K, Soled S, Wold A. Surface acidity and photocatalytic activity of Nb₂O₅/TiO₂ photocatalysts. *J Sol Sta Chem.* 1995; 115:187–91.
- [18] Mozia S. Photocatalytic membrane reactors (PMRs) in water and wastewater treatment: A review. *Sep Purif Technol.* Elsevier B.V. 2010;73(2):71–91.
- [19] Buscio V, Brosillon S, Mendret J, Crespi M, Gutiérrez-Bouzán C. Photocatalytic membrane reactor for the removal of CI disperse Red 73. *Materials.* 2015;8(6):3633–47.
- [20] Kakuta N, White JM, Campion A, Bard AJ, Fox MA, Webber SE. Surface analysis of semiconductor incorporated polymer systems. 1. Nafion and cadmium sulfide-Nafion. *J Phys Chem.* 1985;89:48–52.
- [21] Tsydenov DE, Parmon VN, Vorontsov AV. Toward the design of asymmetric photocatalytic membranes for hydrogen production: Preparation of TiO₂-based membranes and their properties. *Int J Hydrogen Energy.* 2012;37(15):11046–60.
- [22] Hong HJ, Sarkar SK, Lee BT. Formation of TiO₂ nano fibers on a micro-channeled Al₂O₃-ZrO₂/TiO₂ porous composite membrane for photocatalytic filtration. *J Eur Ceram Soc.* 2012;32(3):657–63.

- [23] Rogé V, Bahlawane N, Lamblin G, Fehete I, Garin F, Dinia A, et al. Improvement of the photocatalytic degradation property of ZnO atomic layer deposition thin films: Interplay between film properties and functional performances. *J Mater Chem A*. 2015;3:11453–61.
- [24] Rogé V, Georgantzopoulou A, Mehennaoui K. Tailoring the optical properties of ZnO nano-layers and their effect on in vitro biocompatibility. *RSC Adv*. 2015;97635–47.
- [25] Lee SM, Grass G, Kim GM, Dresbach, Zhang, Gösele U, Knez M. Low-temperature ZnO atomic layer deposition on biotemplates: Flexible photocatalytic ZnO structures from eggshell membranes. *Phys Chem Chem Phys*. 2009;11(19):3607.
- [26] Kim SH, Kwak SY, Sohn BH, Park TH. Design of TiO₂ nanoparticle self-assembled aromatic polyamide thin-film-composite (TFC) membrane as an approach to solve biofouling problem. *J Memb Sci*. 2003;211(1):157–65.
- [27] Rahimpour A, Madaeni SS, Taheri AH, Mansourpanah Y. Coupling TiO₂ nanoparticles with UV irradiation for modification of polyethersulfone ultrafiltration membranes. *J Memb Sci*. 2008;313(1–2):158–69.
- [28] Mansourpanah Y, Madaeni SS, Rahimpour A, Farhadian A, Taheri AH. Formation of appropriate sites on nanofiltration membrane surface for binding TiO₂ photo-catalyst: Performance, characterization and fouling-resistant capability. *J Memb Sci*. 2009;330(1–2):297–306.
- [29] Rahimpour A, Jahanshahi M, Rajaeian B, Rahimnejad M. TiO₂ entrapped nano-composite PVDF/SPES membranes: Preparation, characterization, antifouling and antibacterial properties. *Desalination*. 2011;278(1–3):343–53.
- [30] Leong S, Razmjou A, Wang K, Hapgood K, Zhang X, Wang H. TiO₂ based photocatalytic membranes: A review. *J Memb Sci*. 2014;472:167–84.
- [31] Wang H, Zhang L, Chen Z, Hu J, Li S, Wang Z, et al. Semiconductor heterojunction photocatalysts: design, construction, and photocatalytic performances. *Chem Soc Rev*. 2014;43(15):5234–44.
- [32] Dutta SK, Mehetor SK, Pradhan N. Metal semiconductor heterostructures for photocatalytic conversion of light energy. *J Phys Chem Lett*. 2015;6(6):936–44.
- [33] Reynal A, Willkomm J, Muresan NM, Lakadamyali F, Planells M, Reisner E, et al. Distance dependent charge separation and recombination in semiconductor/molecular catalyst systems for water splitting. *Chem Commun. Royal Society of Chemistry*. 2014;50:12768–71.
- [34] Berr MJ, Wagner P, Fischbach S, Vaneski A, Schneider J, Sussha AS, et al. Hole scavenger redox potentials determine quantum efficiency and stability of Pt-decorated CdS nanorods for photocatalytic hydrogen generation. *Appl Phys Lett*. 2012;100(22):2014–7.

- [35] Wang C, Wang X, Xu BQ, Zhao J, Mai B, Peng P, et al. Enhanced photocatalytic performance of nanosized coupled ZnO/SnO₂ photocatalysts for methyl orange degradation. *J Photochem Photobiol A Chem.* 2004;168(1-2):47-52.
- [36] Uddin T, Nicolas Y, Toupance T, Servant L, Mu MM, Kleebe H, et al. Nanostructured SnO₂-ZnO heterojunction photocatalysts showing enhanced photocatalytic activity for the degradation of organic dyes. *Inorg Chem.* 2012;51(14):7764-73.
- [37] Cun W, Jincai Z, Xinming W, Bixian M, Guoying S, Ping'an P, et al. Preparation, characterization and photocatalytic activity of nano-sized ZnO/SnO₂ coupled photocatalysts. *Appl Catal B Environ.* 2002;39(3):269-79.
- [38] Huang X, Shang L, Chen S, Xia J, Qi X, Wang X, et al. Type-II ZnO nanorod-SnO₂ nanoparticle heterostructures: Characterization of structural, optical and photocatalytic properties. *Nanoscale.* 2013;5:3828-33.
- [39] Liu Z, Sun DD, Guo P, Leckie JO. An efficient bicomponent TiO₂/SnO₂ nanofiber photocatalyst fabricated by electrospinning with a side-by-side dual spinneret method. *Nano Lett.* 2007;7(4):1081-5.
- [40] Wang C, Shao C, Zhang X, Liu Y. SnO₂ nanostructures-TiO₂ nanofibers heterostructures: Controlled fabrication and high photocatalytic properties. *Inorg Chem.* 2009;48(15):7261-8.
- [41] De Mendonça VR, Lopes OF, Fregonesi RP, Giralddi TR, Ribeiro C. TiO₂-SnO₂ heterostructures applied to dye photodegradation: The relationship between variables of synthesis and photocatalytic performance. *Appl Surf Sci.* 2014;298:182-91.
- [42] Lei JF, Li LB, Shen XH, Du K, Ni J, Liu CJ, et al. Fabrication of ordered ZnO/TiO₂ heterostructures via a templating technique. *Langmuir.* 2013;29(45):13975-81.
- [43] Tian J, Chen L, Yin Y, Wang X, Dai J, Zhu Z, et al. Photocatalyst of TiO₂/ZnO nano composite film: Preparation, characterization, and photodegradation activity of methyl orange. *Surf Coatings Technol [Internet]. Elsevier B.V.;* 2009;204(1-2):205-14. Available from: <http://dx.doi.org/10.1016/j.surfcoat.2009.07.008>.
- [44] Ceylan H, Ozgit-Akgun C, Erkal TS, Donmez I, Garifullin R, Tekinay AB, et al. Size-controlled conformal nanofabrication of biotemplated three-dimensional TiO₂ and ZnO nanonetworks. *Sci Rep.* 2013;3:2306.
- [45] Athauda TJ, Neff JG, Sutherland L, Butt U, Ozer RR. Systematic study of the structure-property relationships of branched hierarchical TiO₂/ZnO nanostructures. *ACS Appl Mater Interfaces.* 2012;4(12):6917-26.
- [46] Chen Z, Zhao J, Yang X, Ye Q, Huang K, Hou C, et al. Fabrication of TiO₂/WO₃ composite nanofibers by electrospinning and photocatalytic performance of the resultant fabrics. *Ind Eng Chem Res.* 2016;55(1):80-5.

- [47] Basu M, Garg N, Ganguli AK. A type-II semiconductor (ZnO/CuS heterostructure) for visible light photocatalysis. *J Mater Chem A*. 2014;2(20):7517–25.
- [48] Zhu L, Hong M, Wei Ho G. Hierarchical assembly of SnO₂/ZnO nanostructures for enhanced photocatalytic performance. *Sci Rep*. Nature Publishing Group; 2015;5:1–11. Article No. 11609.
- [49] Jones MR, Osberg KD, Macfarlane RJ, Langille MR, Mirkin CA. Templated techniques for the synthesis and assembly of plasmonic nanostructures. *Chem Rev*. 2011, 111(6): 3736–827.
- [50] Kelly KL, Coronado E, Zhao LL, Schatz GC. The optical properties of metal nanoparticles: The influence of size, shape, and dielectric environment. *J Phys Chem B*. 2003;107(3):668–77.
- [51] Linic S, Christopher P, Ingram DB. Plasmonic-metal nanostructures for efficient conversion of solar to chemical energy. *Nature Publishing Group*; 2011;10(12):911–21.
- [52] McFarland EW, Tang J. A photovoltaic device structure based on internal electron emission. *Nature*. 2003;421(6923):616–8.
- [53] Zhao G, Kozuka H, Yoko T. Sol–gel preparation and photoelectrochemical properties of TiO₂ films containing Au and Ag metal particles. *Thin Solid Films*. 1996;277(1–2): 147–54.
- [54] Tian Y, Tatsuma T. Mechanisms and applications of plasmon-induced charge separation at TiO₂ films loaded with gold nanoparticles. *J Am Chem Soc*. 2005;127(20):7632–7.
- [55] Furube A, Du L, Hara K, Katoh R, Tachiya M. Ultrafast plasmon-induced electron transfer from gold nanodots into TiO₂ nanoparticles. *J Am Chem Soc*. 2007;129(48): 14852–3.
- [56] Fang Y, Jiao Y, Xiong K, Ogier R, Yang Z-J, Gao S, et al. Plasmon enhanced internal photoemission in antenna-spacer-mirror based Au/TiO₂ nanostructures. *Nano Lett*. 2015;15:4059–65.
- [57] He Y, Basnet P, Hunyadi Murph SE, Zhao Y. Ag nanoparticle embedded TiO₂ composite nanorod arrays fabricated by oblique angle deposition: Toward plasmonic photocatalysis. *ACS Appl Mater Interfaces*. 2013;5:11818–27.
- [58] Linic S, Aslam U, Boerigter C, Morabito M. Photochemical transformations on plasmonic metal nanoparticles. *Nat Mater*. 2015;14(6):567–76.
- [59] Liu F, Lubber EJ, Huck LA, Olsen BC, Buriak JM. Nanoscale plasmonic stamp lithography on silicon. *ACS Nano*. 2015;9(2):2184–93.
- [60] Yan J, Jacobsen KW, Thygesen KS. First-principles study of surface plasmons on Ag(111) and H/Ag(111). *Phys Rev B*. 2011;84:235430-4.

- [61] Zhao L-B, Liu X-X, Zhang M, Liu Z-F, Wu D-Y, Tian Z-Q. Surface plasmon catalytic aerobic oxidation of aromatic amines in metal/molecule/metal junctions. *J Phys Chem C*. 2016;120:944–55.
- [62] Wang S, Riedinger A, Li H, Fu C, Liu H, Li L, Liu T, Tan L, Barthel MJ, Pugliese G, De Donato F, Scotto D'Abbusco M, Meng X, Manna L, Meng H, Pellegrino T. Plasmonic copper sulfide nanocrystals exhibiting near-infrared photothermal and photodynamic therapeutic effects. *ACS Nano*. 2015;9(2):1788–800.
- [63] Govorov AO, Richardson HH. Generating heat with metal nanoparticles. *Nano Today*. 2007;2(1):30–8.
- [64] Boyd D, Greengard L, Brongersma M, El-Naggar MY, Goodwin DG. Plasmon-assisted chemical vapor deposition. *Nano Lett*. 2006;6(11):2592–7.
- [65] Fasciani C, Alejo CJB, Grenier M, Netto-Ferreira JC, Scaiano JC. High-temperature organic reactions at room temperature using plasmon exmixed-citation: Decomposition of dicumyl peroxide. *Org Lett*. 2011;13(2):204–7.
- [66] Verbruggen SW, Keulemans M, Filippousi M, Flahaut D, Van Tendeloo G, Lacombe S, et al. Plasmonic gold–silver alloy on TiO₂ photocatalysts with tunable visible light activity. *Appl Catal B Environ*. 2014;156–157:116–21.
- [67] Yu K, Tian Y, Tatsuma T. Size effects of gold nanoparticles on plasmon-induced photocurrents of gold TiO₂ nanocomposites. *Phys Chem Chem Phys*. 2006;8(46):5417.
- [68] Boerigter C, Campana R, Morabito M, Linic S. Evidence and implications of direct charge exmixed-citation as the dominant mechanism in plasmon-mediated photocatalysis. *Nat Commun*. 2016;7:1–9. Article No. 10545.
- [69] Kochuveedu ST, Jang YH, Kim DH. A study on the mechanism for the interaction of light with noble metal-metal oxide semiconductor nanostructures for various photo-physical applications. *Chem Soc Rev*. 2013;42(21):8467–93.
- [70] Chen Z, Fang L, Dong W, Zheng F, Shena M, Wang J. Inverse opal structured Ag/TiO₂ plasmonic photocatalyst prepared by pulsed current deposition and its enhanced visible light photocatalytic activity. *J Mater Chem A*. 2014;2:824–32.
- [71] Zhang Z, Zhang L, Hedhili MN, Zhang H, Wang P. Plasmonic gold nanocrystals coupled with photonic crystal seamlessly on TiO₂ nanotube photoelectrodes for efficient visible light photoelectrochemical water splitting. *Nano Lett*. 2013;13(1):14–20.
- [72] Zang Y, Yin J, He X, Yue C, Wu Z, Li J, et al. Plasmonic-enhanced self-cleaning activity on asymmetric Ag/ZnO surface-enhanced Raman scattering substrates under UV and visible light irradiation. *J Mater Chem A*. 2014;2(21):7747–53.
- [73] Seh ZW, Liu S, Low M, Zhang S-Y, Liu Z, Mlayah A, et al. Janus Au-TiO₂ photocatalysts with strong localization of plasmonic near-fields for efficient visible-light hydrogen generation. *Adv Mater*. 2012;24(17):2310–4.

- [74] Eom H, Jung J-Y, Shin Y, Kim S, Choi J-H, Lee E, et al. Strong localized surface plasmon resonance effects of Ag/TiO₂ core-shell nanowire arrays in UV and visible light for photocatalytic activity. *Nanoscale*. 2014;6(1):226–34.
- [75] Duan H, Xuan Y. Enhanced optical absorption of the plasmonic nanoshell suspension based on the solar photocatalytic hydrogen production system. *Appl Energy*. 2014;114:22–9.
- [76] Hao Q, Wang C, Huang H, Li W, Du D, Han D, et al. Aluminum plasmonic photocatalysis. *Sci Rep*. Nature Publishing Group. 2015;5:1–7. Article No. 15288.
- [77] Karg M, König TAF, Retsch M, Stelling C, Reichstein PM, Honold T, et al. Colloidal self-assembly concepts for light management in photovoltaics. *Mater Today*. 2015;18(4):185–205.
- [78] Pastorelli F, Bidault S, Martorell J, Bonod N. Self-assembled plasmonic oligomers for organic photovoltaics. *Adv Opt Mater*. 2014;2(2):171–5.
- [79] Chong MN, Jin B, Chow CWK, Saint C. Recent developments in photocatalytic water treatment technology: A review. *Water Res*. 2010;44(10):2997–3027.
- [80] Linsebigler AL, Linsebigler AL, Yates Jr JT, Lu G, Lu G, Yates JT. Photocatalysis on TiO₂ surfaces: principles, mechanisms, and selected results. *Chem Rev*. 1995;95(3):735–58.
- [81] Marschall R. Semiconductor composites: Strategies for enhancing charge carrier separation to improve photocatalytic activity. *Adv Funct Mater*. 2014;24:2421–40.
- [82] Ganguly A, Anjaneyulu O, Ojha K, Ganguli AK. Oxide-based nanostructures for photocatalytic and electrocatalytic applications. *CrystEngComm*. Royal Society of Chemistry. 2015;17(47):8978–9001.
- [83] Kudo A, Miseki Y. Heterogeneous photocatalyst materials for water splitting. *Chem Soc Rev*. 2009;38(1):253–78.
- [84] Kadowaki H, Saito N, Nishiyama H, Inoue Y. RuO₂-loaded Sr²⁺-doped CeO₂ with d⁰ electronic configuration as a new photocatalyst for overall water splitting. *Chem Lett*. 2007;36:440–441.
- [85] Lu X, Zhai T, Cui H, Shi J, Xie S, Huang Y, et al. Redox cycles promoting photocatalytic hydrogen evolution of CeO₂ nanorods. *J Mater Chem*. 2011;21(15):5569.
- [86] Tang Z-R, Zhang Y, Xu Y-J. A facile and high-yield approach to synthesize one-dimensional CeO₂ nanotubes with well-shaped hollow interior as a photocatalyst for degradation of toxic pollutants. *RSC Adv*. 2011;1(9): 1772–7.
- [87] Stranks SD, Snaith HJ. Metal-halide perovskites for photovoltaic and light-emitting devices. *Nat Nanotechnol*. Nature Publishing Group. 2015;10(5):391–402.

- [88] Zhang K, Sunarso J, Shao Z, Zhou W, Sun C, Wang S, et al. Research progress and materials selection guidelines on mixed conducting perovskite-type ceramic membranes for oxygen production. *RSC Adv.* 2011;1(9):1661–76.
- [89] Grewe T, Tüysüz H. Amorphous and crystalline sodium tantalate composites for photocatalytic water splitting. *ACS Appl Mater Interfaces.* 2015;7(41):23153–62.
- [90] Yin S, Tian H, Ren Z, Wei X, Chao C, Pei J, et al. Octahedral-shaped perovskite nanocrystals and their visible-light photocatalytic activity. *Chem Commun.* 2014;50(45):6027–30.
- [91] Tanaka H, Misono M. Advances in designing perovskite catalysts. *Curr Opin Solid State Mater Sci.* 2001;5(5):381–7.
- [92] Grabowska E. Selected perovskite oxides: Characterization, preparation and photocatalytic properties—a review. *Appl Catal B Environ.* 2015;186:97–126.
- [93] Jingshan L, Jeong-Hyeok I, Mayer MT, Schreier M, Nazeeruddin MK, Nam-Gyu P, et al. Water photolysis at 12.3% efficiency via perovskite photovoltaics and Earth-abundant catalysts. *Science.* 2014;345:1593–6.
- [94] Chan SHS, Wu TY, Juan JC, Teh CY. Recent developments of metal oxide semiconductors as photocatalysts in advanced oxidation processes (AOPs) for treatment of dye waste-water. *J Chem Technol Biotechnol.* 2011;86(9):1130–58.
- [95] Naresh G, Mandal TK. Excellent sun-light-driven photocatalytic activity by aurivillius layered perovskites, $\text{Bi}_{5-x}\text{La}_x\text{Ti}_3\text{FeO}_{15}$ ($x = 1, 2$). *ACS Appl Mater Interfaces.* 2014;6(23):21000–10.
- [96] Wu W-Q, Feng H-L, Rao H-S, Xu Y-F, Kuang D-B, Su C-Y. Maximizing omnidirectional light harvesting in metal oxide hyperbranched array architectures. *Nat Commun.* Nature Publishing Group. 2014;5:1–9. Article No. 3968.
- [97] Li L, Yan J, Wang T, Zhao Z-J, Zhang J, Gong J, et al. Sub-10 nm rutile titanium dioxide nanoparticles for efficient visible-light-driven photocatalytic hydrogen production. *Nat Commun.* Nature Publishing Group. 2015;6:1–10. Article No. 5881.
- [98] Tan C, Zhang H. Wet-chemical synthesis and applications of non-layer structured two-dimensional nanomaterials. *Nat Commun.* Nature Publishing Group. 2015;6:1–13.
- [99] Zhou Y, Zhang Y, Lin M, Long J, Zhang Z, Lin H, et al. Monolayered Bi_2WO_6 nano-sheets mimicking heterojunction interface with open surfaces for photocatalysis. *Nat Commun.* Nature Publishing Group. 2015;6,8340:1–8.